



A brief review of atomic layer deposition: from fundamentals to applications

Richard W. Johnson^{1,3}, Adam Hultqvist^{2,3} and Stacey F. Bent^{1,2,*}

¹Department of Materials Science and Engineering, Stanford University, Stanford, CA 94305, USA

²Department of Chemical Engineering, Stanford University, Stanford, CA 94305, USA

Atomic layer deposition (ALD) is a vapor phase technique capable of producing thin films of a variety of materials. Based on sequential, self-limiting reactions, ALD offers exceptional conformality on high-aspect ratio structures, thickness control at the Angstrom level, and tunable film composition. With these advantages, ALD has emerged as a powerful tool for many industrial and research applications. In this review, we provide a brief introduction to ALD and highlight select applications, including Cu(In,Ga)Se₂ solar cell devices, high-k transistors, and solid oxide fuel cells. These examples are chosen to illustrate the variety of technologies that are impacted by ALD, the range of materials that ALD can deposit – from metal oxides such as Zn_{1-x}Sn_xO_y, ZrO₂, Y₂O₃, to noble metals such as Pt – and the way in which the unique features of ALD can enable new levels of performance and deeper fundamental understanding to be achieved.

Introduction

Atomic layer deposition (ALD) is a technique capable of depositing a variety of thin film materials from the vapor phase. ALD has shown great promise in emerging semiconductor and energy conversion technologies. This review is intended to introduce the reader to the basics of ALD and highlight current applications pertaining to microelectronics and energy that were selected because of their importance in either industry or research. For a more comprehensive summary of ALD and its many applications, the reader is referred to existing reviews on the topic [1–10].

As device requirements push toward smaller and more spatially demanding structures, ALD has demonstrated potential advantages over alternative deposition methods, such as chemical vapor deposition (CVD) and various physical vapor deposition (PVD) techniques, due to its conformality and control over materials thickness and composition. These desirable characteristics originate from the cyclic, self-saturating nature of ALD processes.

ALD was popularly introduced as atomic layer epitaxy (ALE) by Suntola and Antson in 1977, depositing ZnS for flat panel displays

[11]. As further ALE processes were developed to incorporate metals and metal oxides, many materials were deposited non-epitaxially and the more general name of ALD was adopted to reflect this [1]. It should be noted, too, that many ALD procedures were developed from a variety of CVD processes. In contrast to their CVD analogs, the ALD procedures feature alternating exposure of chemical precursors to react to form the desired material, often at significantly lower temperatures [12].

A general ALD process is illustrated in Fig. 1. It consists of sequential alternating pulses of gaseous chemical precursors that react with the substrate. These individual gas-surface reactions are called ‘half-reactions’ and appropriately make up only part of the materials synthesis. During each half-reaction, the precursor is pulsed into a chamber under vacuum (<1 Torr) for a designated amount of time to allow the precursor to fully react with the substrate surface through a self-limiting process that leaves no more than one monolayer at the surface. Subsequently, the chamber is purged with an inert carrier gas (typically N₂ or Ar) to remove any unreacted precursor or reaction by-products. This is then followed by the counter-reactant precursor pulse and purge, creating up to one layer of the desired material. This process is then cycled until the appropriate film thickness is achieved. Typically,

*Corresponding author: Bent, S.F. (sbent@stanford.edu)

³ authors contributed equally.

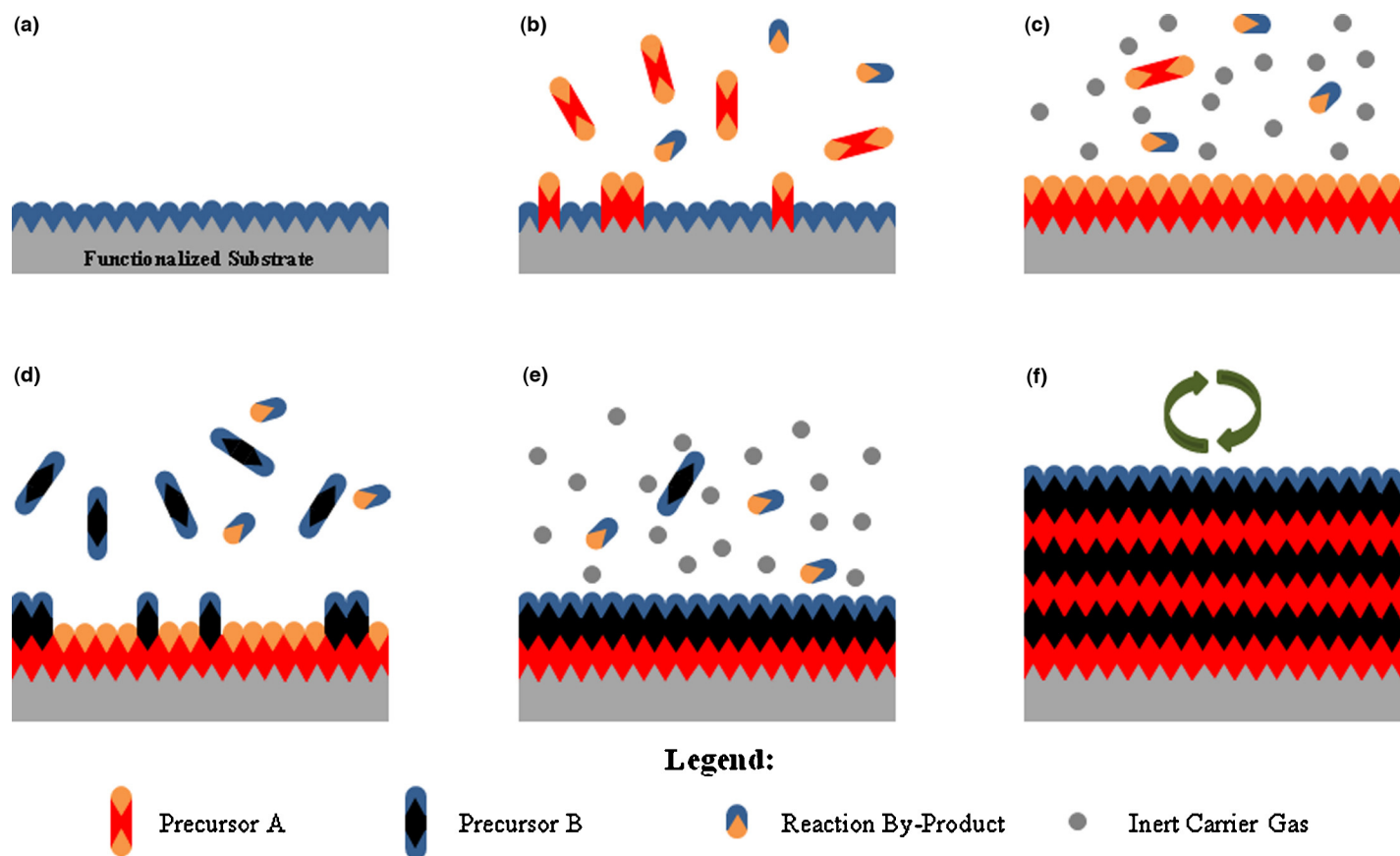


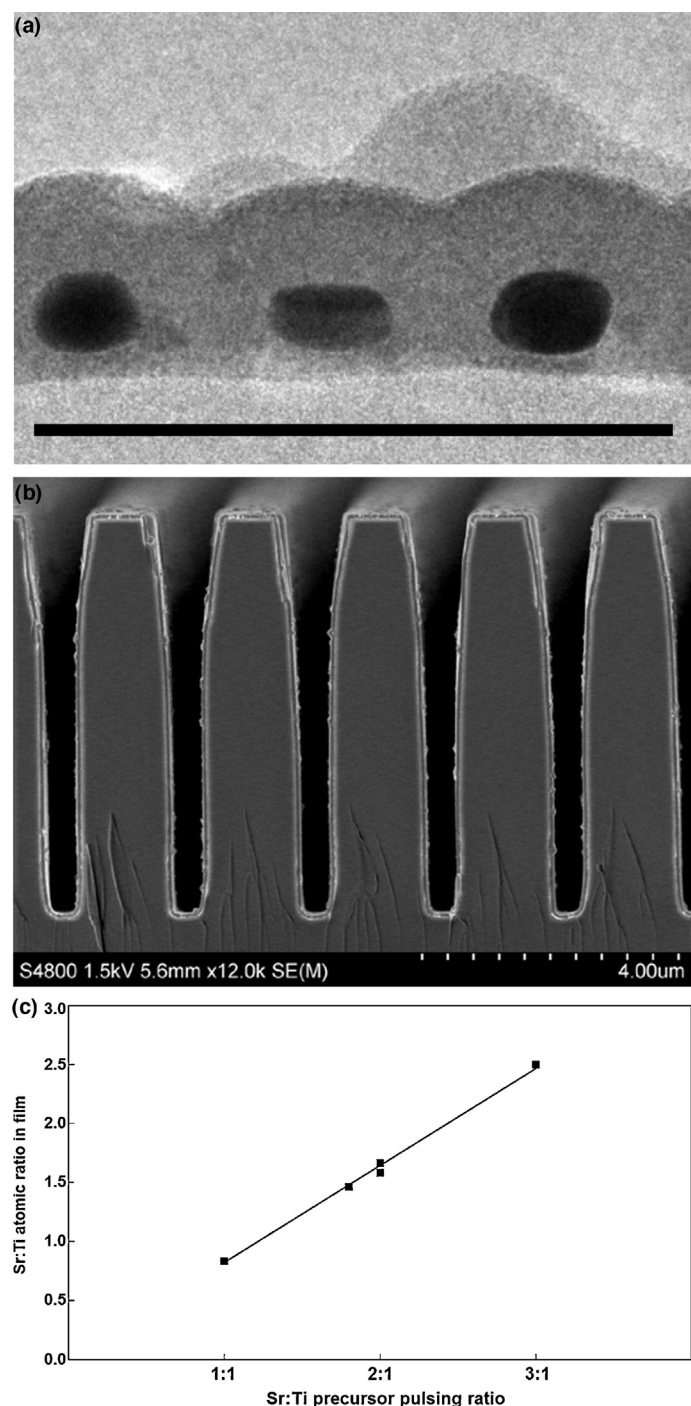
FIGURE 1

Schematic of ALD process. (a) Substrate surface has natural functionalization or is treated to functionalize the surface. (b) Precursor A is pulsed and reacts with surface. (c) Excess precursor and reaction by-products are purged with inert carrier gas. (d) Precursor B is pulsed and reacts with surface. (e) Excess precursor and reaction by-products are purged with inert carrier gas. (f) Steps 2–5 are repeated until the desired material thickness is achieved.

ALD processes are conducted at modest temperatures ($<350\text{ }^{\circ}\text{C}$). The temperature range where the growth is saturated depends on the specific ALD process and is referred to as the ‘ALD temperature window’. Temperatures outside of the window generally result in poor growth rates and non-ALD type deposition due to effects such as slow reaction kinetics or precursor condensation (at low temperature) and thermal decomposition or rapid desorption of the precursor (at high temperature). In order to benefit from the many advantages of ALD, it is desirable to operate within the designated ALD window for each deposition process.

The primary advantages of ALD are all derived from the sequential, self-saturating, gas-surface reaction control of the deposition process. Firstly, the conformality of ALD-deposited films is often the critical factor in choosing ALD over competing deposition techniques such as CVD or sputtering. Conformality of high aspect ratio and three dimensionally-structured materials is made possible by its self-limiting characteristic, which restricts the reaction at the surface to no more than one layer of precursor. With sufficient precursor pulse times, the precursor can disperse into deep trenches, allowing for complete reaction with the entire surface. Subsequent cycles allow for uniform growth on high aspect ratio structures, whereas CVD and PVD may suffer from non-uniformity due to faster surface reactions and shadowing effects, respectively. Examples of the superior conformality of ALD films are shown in Fig. 2a and b for SnS_x films on Au nanoparticles and $\text{Ge}_2\text{Sb}_2\text{Te}_5$ films over SiO_2 trenches; the ability of the process to evenly coat

the substrate morphology is evident. A second apparent advantage of ALD is the thickness control of the deposited thin films. By utilizing layer-by-layer deposition, the thickness of a film can be tailored by the number of ALD cycles. Growth per cycle for many ALD films has been summarized in previous reviews [1,2] and is typically less than one $\text{\AA}/\text{cycle}$, depending on the individual process. Another prominent advantage of ALD is composition control. Composition control has been demonstrated with materials such as zinc tin oxide (ZTO) [13] and SrTiO_3 [14], among many others [15–17]. These films can be deposited and compositionally controlled by tailoring ALD ‘super cycles’, which are composed of multiple ALD processes. For example, in ZTO deposition, adjusting the super cycle ratios for SnO_x and ZnO can tailor different conduction behavior and optical properties of the film [13]. In depositing SrTiO_3 , ALD processes for TiO_2 and SrCO_3 are alternated in a super cycle at a 1:1 ratio, producing a stoichiometric SrTiO_3 film after annealing (Fig. 2) [14]. However, it should be noted that a nonlinear relationship between the cycle ratio and the film’s atomic ratio is common for the ternary oxide processes [16,17], making it less straightforward to deposit a film with a certain desired composition. For example, additional studies on SrTiO_3 , ALD have indicated that a 1:1 Sr:Ti atomic ratio in films is also possible for ALD cycle ratios between 0.67 and 0.82 [15]. Other complications in composition control for ternary and quaternary metal oxide ALD arise from the need for the growth windows of individual ALD processes to be thermally compatible and the way

**FIGURE 2**

Examples of ALD strengths. (a) TEM image of conformal SnS_x ALD film on Au nanoparticles. Scale bar is 100 nm. (b) SEM cross-sectional image of conformal Ge₂Sb₂Te₅ ALD film in trenches [30]. (c) SrTiO₃ stoichiometry as a function of SrCO₃ and TiO₂ ALD super cycle ratio [14]. Image (b) Reprinted with permission from Ref. [30]. Copyright (2009) American Chemical Society and image (c) Reprinted (adapted) from Ref. [14], Copyright (2003), with permission from Elsevier.

in which ALD introduces dopants into the films as ‘δ-doping’ spikes resulting in inhomogeneous films as-deposited that typically require annealing [18].

While ALD has many promising features, it also suffers from slow deposition rates. Because of the long cycle times involved in pulsing and purging precursors and the layer-by-layer nature of the

deposition, most ALD rates are on the order of 100–300 nm/h [3,12]. This rate is strongly dependent on the reactor design and the aspect ratio of the substrate, however. As the surface area and volume of an ALD reactor increase, so does the time needed for pulsing and purging. High aspect ratio substrates also require longer pulse and purge times to allow for the precursor gas to disperse into trenches and other three dimensional features. To combat this shortcoming, spatial ALD has emerged as a promising technique that may significantly improve throughput [19–23]. Spatial ALD operates by eliminating the traditional pulse/purge chamber and replacing it with a spatially-resolved head, which exposes the substrate to a specific gas precursor based on location. In one design, as the head translates around the substrate, it alters the exposed precursor, resulting in film growth. Alternatively, spatial ALD has also been demonstrated in which the substrate moves past stationary precursor nozzles, which are arranged so that by passing by them, precursor cycling is achieved and the film is grown. Overall, with spatial ALD techniques, deposition rates around 3600 nm/h are possible [24].

A wide range of materials has been grown by ALD in previous studies [1,4–10]. The materials encompass metals, insulators and semiconductors in both crystalline and amorphous phases. In addition, ALD offers a large selection of elements to choose from to create the material of choice, as listed in Table 1 [5,25–30]. This table shows that the most common types of ALD-grown materials so far are oxides, nitrides, sulfides and pure elements. Despite their more complex ALD process, compounds with three or more elements have also recently gained much interest due to their desirable materials properties and will therefore be showcased with a few examples in this review.

While the selection of materials listed in Table 1 is impressive, it clearly also shows that it is not yet possible to grow every material by ALD. The main limit of the availability of a material by ALD is the limited choice of effective reaction pathways. The selection is further limited by the availability of reactants that can facilitate the appropriate reaction pathway. As discussed earlier, it is desirable to run the ALD process in a self-limiting growth regime. This imposes a list of requirements on the reactants. Foremost, a reactant and counter reactant that will deposit the desired material must be available or synthesized. In some cases, the selection of available reactants for a given element is very limited or non-existent. The reactants should be volatile enough to be in the gas phase either at room temperature or upon moderate heating. Furthermore, while in the gas phase they should not decompose until they have reached and reacted with the sample surface. The surface reaction should preferably be quick and irreversible to lead to fast growth saturation. Neither the reactant nor its by-products, after reacting with the surface, should dissolve, etch or in other ways damage the substrate, the growing film or the ALD reactor itself. It is also preferable if the reactants are small in size to avoid reduced surface coverage due to steric hindrance. Finally, the choice of reactants has economic implications, as some are expensive and synthesis can be time consuming. Unfortunately, there are no perfect reactants, so the choice of reagents typically involves making tradeoffs between cost, availability, safety, volatility and reactivity.

There are two main groups of metal reactants: inorganic, as in the elemental and the metal halides, and metal organic, as in

TABLE 1

List of materials grown by ALD [5,25–30].

Elemental	Oxides	Nitrides	Sulfides	Other compounds
C, Al, Si, Ti, Fe, Co, Ni, Cu, Zn, Ga, Ge, Mo, Ru, Rh, Pd, Ag, Ta, W, Os, Ir, Pt	Li, Be, B, Mg, Al, Si, P, Ca, Sc, Ti, V, Cr, Mn, Fe, Co, Ni, Cu, Zn, Ga, Ge, Sr, Y, Zr, Nb, Ru, Rh, Pd, In, Sn, Sb, Ba, La, Ce, Pr, Nd, Sm, Eu, Gd, Tb, Dy, Ho, Er, Tm, Yb, Lu, Hf, W, Ir, Pt, Pb, Bi	B, Al, Si, Ti, Cu, Ga, Zr, Nb, Mo, In, Hf, Ta, W	Ca, Ti, Mn, Cu, Zn, Sr, Y, Cd, In, Sn, Sb, Ba, La, W	Li, B, Mg, Al, Si, P, Ca, Ti, Cr, Mn, Co, Cu, Zn, Ga, Ge, As, Sr, Y, Cd, In, Sb, Te, Ba, La, Pr, Nd, Lu, Hf, Ta, W, Bi

TABLE 2

Available reactant groups for specific elements [4,25–30].

Elemental	Halides	Alkyls	Cyclopentadienyls	β -diketonates	Other reactants
Mg, Mn, Zn, Ga, Cd, In, Sn	B, C, Ti, V, Cr, Mn, Cu, Zn, Ga, Ge, Zr, Nb, Mo, Cd, In, Sn, Sb, Hf, Ta, W, Pb	Be, Al, Si, Zn, Ga, Ge, Cd, In, Sn, Hg	Mg, Sc, Ni, Sr, Y, Zr, Ru, Lu, Os, Pt	Mg, Ca, Sc, V, Cr, Mn, Fe, Co, Ni, Cu, Ga, Sr, Y, Zr, Ru, Pd, In, Ba, La, Ce, Nd, Sm, Eu, Gd, Tb, Dy, Ho, Er, Tm, Ir, Pt, Pb	Li, P, Ti, Fe, Co, Ni, Cu, Zn, Ge, As, Zr, Rh, Ag, Sb, Te, La, Pr, Yb, Hf, Ta, W, Ir, Pt, Pb, Bi

alkyls, cyclopentadienyls, alkoxides, β -diketonates, amides, silyls and amidinates [4,5]. Here we describe some of the benefits and challenges associated with each type of precursor. Elemental reactants grow materials that are free of contamination and their growth is not reduced by steric hindrance, but there is only a small selection of metals that have a high enough vapor pressure to be suitable as elemental reactants. Halides are very reactive, have low steric hindrance and can be used in a wide temperature range, but suffer from having reactive by-products and from unintentional incorporation of the halide atoms into the growing material. Alkyls are also very reactive due to the direct metal carbon bond and can use H₂O as a counter reactant, but are limited by decomposition at higher temperatures and are only available for a small number of elements. Similarly, the cyclopentadienyls are reactive due to their metal carbon bonds and can use water as a counter reactant, but suffer from decomposition at higher temperatures and are only available for a small number of elements. In contrast, β -diketonates exist for a large variety of elements, but are bulky and have low reactivity leading to low growth rates. They also require more reactive counter reactants such as O₃ to achieve their highest oxide growth rates. Alkoxides suffer mainly from poor thermal stability. Amides and silyls show good reactivity, but decompose at quite low temperatures. Amidinates are a promising alternative for the future, as they are projected to be available for a big group of elements, and have decent thermal stability and good reactivity. Due to these tradeoffs and the limited choice for each element, research into new reactants is continually ongoing [5,9]. Table 2 lists the reactant groups that are currently available for a given element [4,25–30].

There is also a selection of counter reactants that are appropriately suited to the metal reactants. For instance, oxygen counter reactants include H₂O, O₃, O₂, H₂O₂, and O• from a plasma source [4,5]. Creating highly reactive radicals from a plasma source is a relatively new concept in ALD that is commonly denoted as plasma enhanced ALD (PEALD) [1,5–7]. While O₃ and O• are very reactive and therefore can use lower deposition temperatures and enable the use of less reactive metal reactants, they are also more likely to oxidize the surface of the underlying substrate and create an unwanted interfacial layer [29–31]. Despite being less reactive,

H₂O is most commonly used for oxides, since it is gentler to the substrate surface and can withstand higher deposition temperatures without decomposing. For similar reasons, other hydrides such as NH₃ and H₂S are commonly used as counter reactants for nitrides and sulfides, respectively [4,5]. In rare cases even H₂Se is used to grow selenides, despite its toxicity [4,5].

In the following sections of this review, we will showcase some of the latest and most exciting applications of ALD. We have selected field effect transistors, thin film solar cells, and fuel cells to highlight here, because these applications each show how the unique features of ALD enable new levels of performance and deeper fundamental understanding to be achieved. These examples also illustrate the range of materials that ALD can deposit. Finally, the selection was made to show that different scientific and engineering problems can be solved by ALD, both in industry and on a research scale. In short, we hope that these applications will convince the reader that ALD is a powerful tool for solving material science problems.

ALD in microelectronics: high-k gate dielectrics

The microelectronics industry is one of the biggest adopters of ALD. Even in the late 1990s, Samsung was experimenting with ALD for improving the storage capacitor in DRAM memories [32]. In current transistor fabrication, research and development rely on using ALD for depositing pinhole-free, conformal films with well-controlled thickness and a high dielectric constant [33,34].

As industry has transitioned to the use of high-k dielectrics for the transistor gate stack in microelectronics devices, ALD has become increasingly important. The high-k gate oxides need to be highly uniform and pinhole-free on Si to prevent leakage current through the gate oxide. To solve the oxide thickness reduction challenges, Intel introduced ALD into their mass production line in 2007 [34]. This was a key reason they were able to advance from the 65 nm to the 45 nm node technology without creating transistors with significantly higher power consumption. The oxide layer they used consisted of a stack of layers: a SiON interfacial layer to electrically passivate the Si surface, a high-k HfO₂ based oxide with a *k*-value of around 20, and a capping layer to match the work function of the gate metal [35]. Shortly

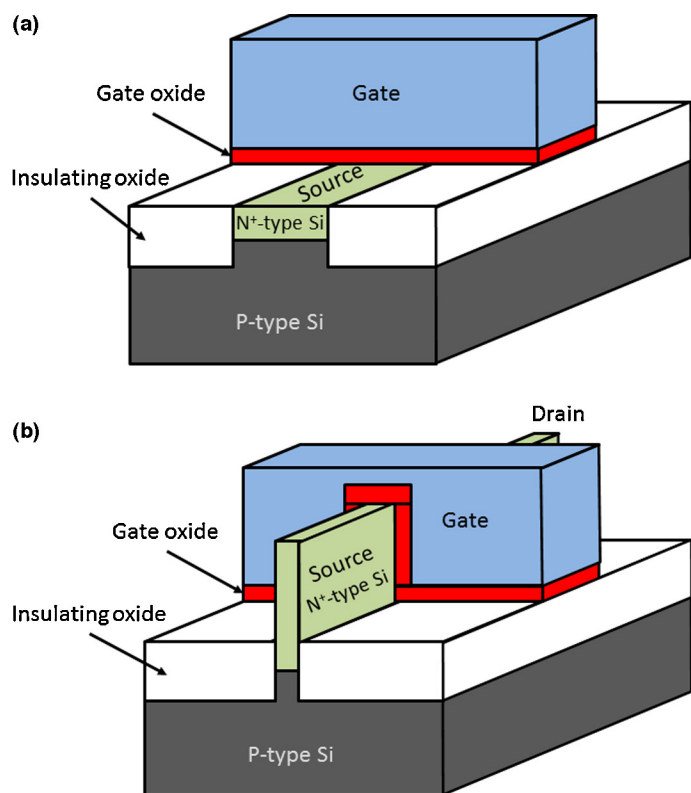


FIGURE 3

(a) The traditional planar MOSFET design leading to an inverted surface channel and (b) the FinFET or tri-gate design where a Si fin that is covered by the gate oxide from three sides becomes inverted from the surrounding gate oxide, thus increasing the overall inverted volume compared to the planar design for the same gate voltage.

afterward, other major players in the semiconductor industry followed suit and started their own production using ALD to deposit high-*k* dielectrics [36–39].

As the devices have continued to shrink, in part enabled by the ALD gate oxides which decreased the equivalent gate oxide thickness, new limitations on the bulk Si crystal have forced the industry to look for other, more radical alternatives to the traditional transistor concept. In their latest technology, the 22 nm node [33], Intel introduced a structure called tri-gate into production, which is a variant of the Fin field effect transistor (FinFET) structure. Instead of using the traditional planar channel, shown in Fig. 3a, where only the top of the Si bulk crystal is inverted, this new structure has fin like slabs of Si sticking out of the bulk crystal, as shown in Figs. 3b and 4a.

In this tri-gate design, the high aspect ratio fins protruding from the surface need to be covered with a gate oxide of great compositional and thickness uniformity and without pinholes, a task tailored for ALD. One can speculate whether such a non-planar structure would have been so readily implemented into fabrication were it not for the conformal ALD gate oxides already being a part of the existing production line.

Although information on what will be implemented by the chipmakers in the next generation technology is not public, it is informative to look toward some of the topics that are currently being researched by universities or institutes. One idea is to use the conformal ALD gate oxides and continue along the FinFET track

and further encompass the gate by undercutting it a bit on the fourth side, creating an omega gate [40], as shown in Fig. 4b. Another version is to cover the fin even below the bulk crystal surface level creating a pi gate [41] depicted in Fig. 4c. The ultimate design would be to use a semiconducting wire or tube and completely surround it by the gate [42] like the nanotube in Fig. 4d. These device structures are clearly enabled by the conformality of a process like ALD.

Another idea being pursued is to find a gate oxide for Si which has an even higher dielectric constant and which can be deposited by ALD. Possible candidates include SrTiO₃ [43], Al-doped TiO₂ [44], LaLuO₃ [45], Hf_{1-x}Zr_xO₂ [46], SrRuO₃ [47] and HfTiO_x [48]. Once again, ALD turns out to be an excellent tool to explore new high-*k* compounds due to its ability to grow compositionally-uniform films and its relatively straightforward way of controlling the material composition by alternating binary material cycles during growth.

Lastly, to reduce the power and to increase the speed of the devices, it is of interest to increase the electron and hole mobility within the channel for the NMOS and p-channel MOSFET (PMOS) transistors respectively. It is therefore natural to look toward alternative semiconductors to bulk silicon in which the electron or hole mobility is higher. III-V compound semiconductors are generally good examples of materials with excellent electron mobility, whereas Ge is an example of a material with an excellent hole mobility. The FinFET structure has the same advantages for these materials as well [49–51], but will require new high-*k* dielectric gate stacks that are adapted to these materials instead. Materials such as TaSiO_x, HfO₂, Al₂O₃ and HfAlO have so far successfully been implemented as high-*k* dielectrics by ALD for III-V compounds [52,53] and Al₂O₃ and HfO₂ for Ge [49,50,54]. It also is critical to form a good passivation layer on top of Ge [55] and to rid the III-V/high-*k* dielectric interface of native surface oxides that tend to pin the Fermi level at the interface [56]. Interestingly enough, certain ALD precursors as TMA have shown the ability to remove all or some of these native oxides during the ALD process [55]. This is yet another advantage that hints at ALD being an important tool for the future of electronics development.

Looking further ahead, ALD promises to be an interesting technique for applications in emerging electronics where new, lower dimensionality semiconductors using sheet, tube or wire based structures such as graphene [57], WSe₂ [58], carbon nanotubes [59] and semiconductor nanowires [60] require a conformal high-*k* gate oxide coating that does not significantly disrupt the unique low dimensional material properties. With continued scaling and adoption of new designs and materials, ALD is likely to become an even more critical tool for the microelectronics industry in the future.

ALD in photovoltaics: buffer layers in Cu(In,Ga)Se₂ thin film solar cells

There are numerous applications for ALD in photovoltaic devices [10]. Materials deposited by ALD are used as a rear contact passivation layer [61], in organic solar cells as a means to tune the electrode work function [62], and in dye sensitized solar cells as a barrier to prevent recombination [63]. Additionally, ALD can be used to create the transparent conducting oxide for the solar cell technologies listed above [64]. There is also research on creating

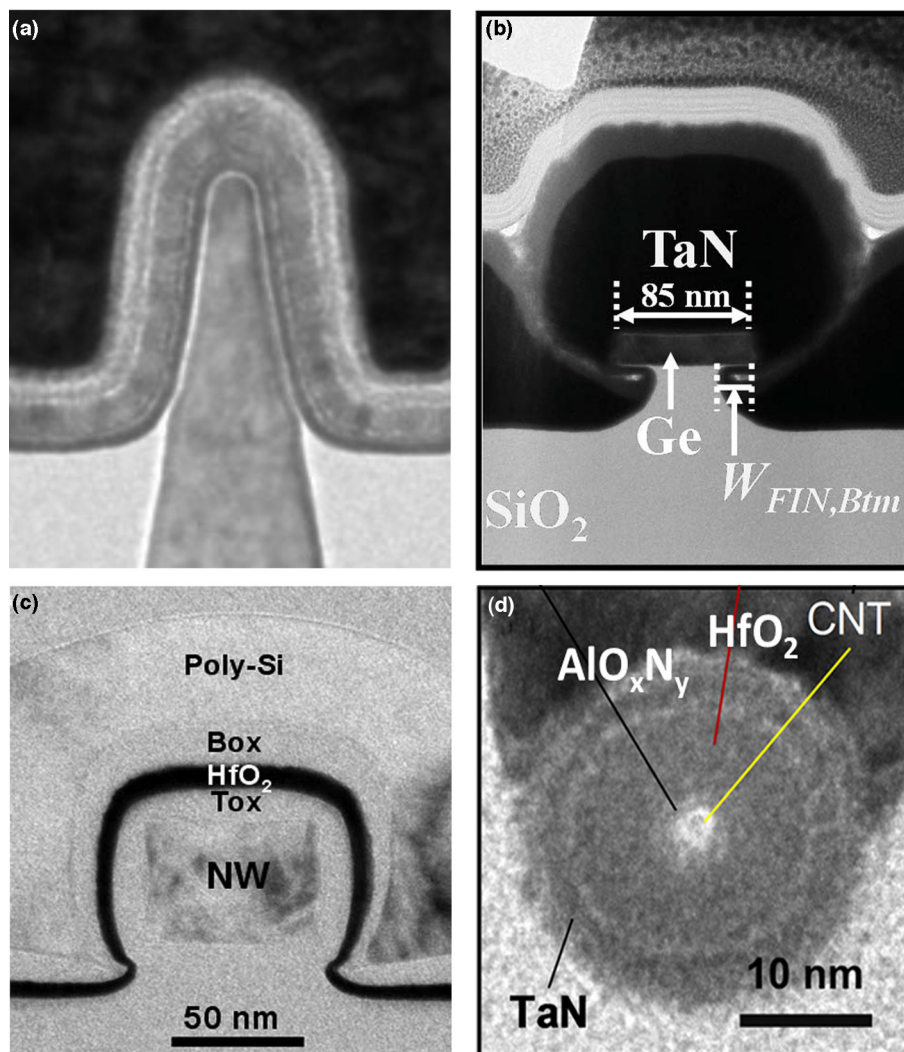


FIGURE 4

Different multiple gate design structures where ALD gate oxides have been used. (a) A TEM cross-section of Intel's [33] FinFET transistor at the 22 nm node with the gate-oxide and gate wrapped around the fin. (b) Liu *et al.* omega gate structure wrapping around a Ge channel [50]. (c) A pi-gate surrounding a poly-Si nanowire in a thin film transistor by Chen *et al.* [60]. (d) A carbon nanotube FET with a gate all around structure by Franklin *et al.* [59]. Reprinted from (a) Copyright (2012) IEEE. Reprinted, with permission, from Ref. [33], (b) Copyright (2013) IEEE. Reprinted, with permission, from Ref. [50], (c) Copyright (2013) IEEE. Reprinted, with permission, from Ref. [60], (d) Reprinted with permission from Ref. [59], Copyright (2013) American Chemical Society.

the light absorbing layer using ALD both in the form of thin films [65] and in the form of nanoparticles with quantum confinement properties [66,67]. Finally, as we will discuss in further detail in this section, it can be used in thin film solar cells to engineer the electrical junction properties of the solar cell diode.

The ability to precisely control the composition of a compound of three or more elements by ALD is very useful in optoelectronic materials such as photovoltaics as it enables a means to controllably vary properties as band gap, density, conductivity, energy band levels, and morphology. An example of this is the ALD-grown $Zn_{1-x}Sn_xO_y$ compound, where the conduction band level and valence band level were found by Kapilashrami *et al.* [68] to change as the composition is varied from ZnO to SnO_y , shown in Fig. 5.

One application where the ability to finely tune the composition and in turn the position of the conduction and valence bands is required is in Cu(In,Ga)Se₂ (CIGS) thin film solar cells. Since CIGS is p-type as deposited, n-type layers of different semiconductors are

introduced in CIGS solar cells to form the electrical pn-junction, as shown in Fig. 6a [69]. The n-type layer deposited directly on top of the CIGS is defined as the buffer layer. Since it forms the pn-junction, the electrical properties of this buffer layer are critical. The standard material for this buffer layer is CdS, but because CdS is toxic and also parasitically absorbs blue light, much research effort has been expended on finding a good alternative. It is believed that a small positive conduction band offset (CBO) toward the CIGS is required for an optimal buffer layer [70]. Finding such a CBO is a task that is inherently well suited for an ALD process in which the material composition can be controlled. Moreover, other ALD benefits are also important for CIGS solar cells. The CIGS surface is typically very uneven, with surface roughness values in the range of 10–100 nm, and crevices can form between grains as shown in the TEM micrograph taken by Lindahl *et al.* [71] in Fig. 6b. It is therefore desirable to use a conformal buffer layer such as the ones obtained by ALD to fully cover the rough CIGS surface. This is especially important during large scale fabrication since the buffer layer must be

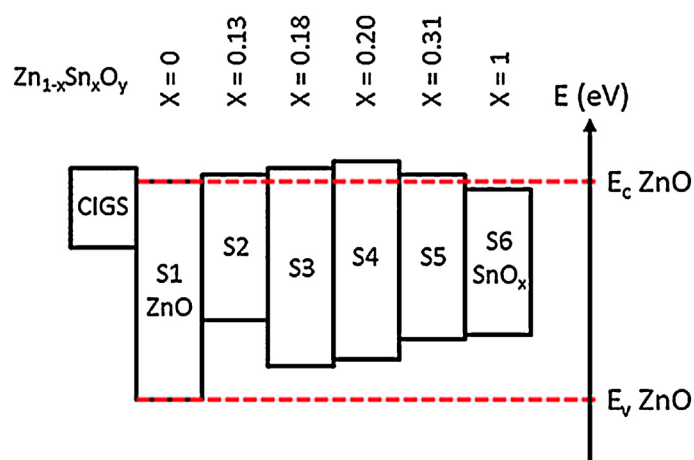


FIGURE 5

Energy band levels of ALD-grown $Zn_{1-x}Sn_xO_y$ as a function of x . The band positions were recently determined by Kapilashrami *et al.* [68] using a combination of X-ray emission spectroscopy and X-ray absorption spectroscopy. Fig. 5 is reprinted from Ref. [68], with permission from the PCCP Owner Societies.

pinhole free over the entire 1 m^2 solar cell module, in order to not severely degrade its performance.

Historically, there has been extensive research on CIGS buffer layers [72], but the binary system ZnO was the first CIGS buffer layer to be deposited by ALD [73]. The performance of the ZnO was found to be lacking, mainly due to high recombination because of the unfavorable CBO. This led to the development of ternary ALD compound systems such as Zn(O,S) [74] and (Zn,Mg)O [75], where the properties of ZnO could be modified so that a more favorable CBO could be achieved. Both of these ALD-grown ternary compounds were later shown to be excellent buffer layer candidates for

CIGS solar cells, each producing devices with power conversion efficiencies of more than 18%, which was comparable to or better than their corresponding reference devices using CdS. In the meantime, the ALD-grown binary compound In_2S_3 showed excellent performance creating CIGS solar cells with over 16% conversion efficiency [76]. Recently, the interest in using ALD for CIGS buffer layers has increased both for improving and understanding [76–82] the systems mentioned above and for developing new materials combinations such as $Zn_{1-x}Sn_xO_y$ [68,71,83] and ZnInS [84].

In a recent experiment by Hultqvist *et al.* [83] the composition of the $Zn_{1-x}Sn_xO_y$ buffer layer in CIGS solar cells was varied in order to find a composition where the CBO was favorable. These results further highlight the strength of ALD in carrying out compositional tuning in materials. Fig. 7 shows the resulting conversion efficiency of the solar cells as a function of the $Zn_{1-x}Sn_xO_y$ composition. From these results it is clear that there are intermediate $Zn_{1-x}Sn_xO_y$ compounds where the solar cell efficiency is higher, mainly due to a high open circuit voltage (V_{oc}), which is an indirect indicator of a small recombination current. Thus, by tuning the $Zn_{1-x}Sn_xO_y$ composition and in turn the conduction band level, a favorable CBO with reduced recombination is found for a composition of approximately $x = 0.2$. A more recent study by Lindahl *et al.* [71] showed that it was possible to push the performance of the CIGS solar cells above 18% using the right $Zn_{1-x}Sn_xO_y$ composition and thickness. This same study [71] also demonstrated that the performance of the solar cells using sufficiently thick $Zn_{1-x}Sn_xO_y$ buffer layers could be retained even if the intrinsic-ZnO layer, typically deposited to prevent shunts, was thinned or completely omitted from the CIGS solar cell stack. This reduction of a processing step, enabled by the pinhole-free, conformal coating properties of ALD, could potentially reduce the manufacturing costs of CIGS modules.

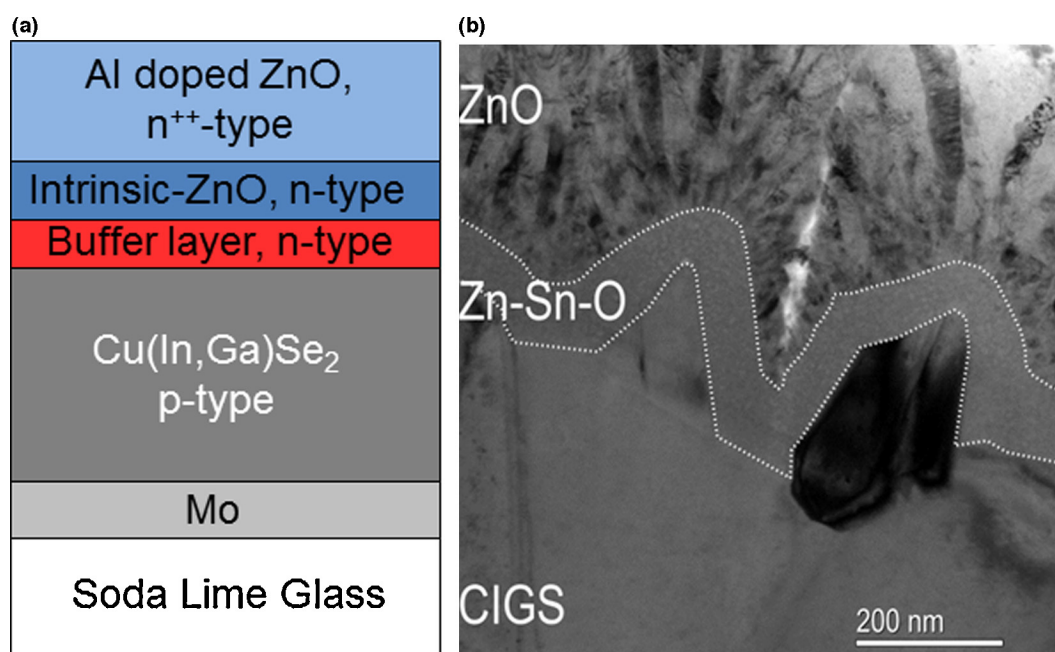


FIGURE 6

(a) Conceptual CIGS solar cell stack and (b) the corresponding TEM cross section, where the CIGS layer has a conformal coating of ALD $Zn_{1-x}Sn_xO_y$ [71]. To more easily distinguish between the layers in the TEM micrograph, a dotted line has been added to define the CIGS/ $Zn_{1-x}Sn_xO_y$ and $Zn_{1-x}Sn_xO_y$ /intrinsic ZnO interfaces. Fig. 6 is reprinted from Ref. [71], Copyright (2012) John Wiley & Sons Ltd.

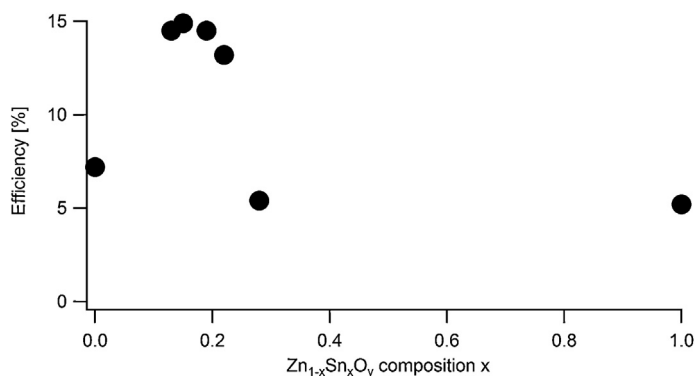


FIGURE 7

Measured solar cell conversion efficiency as a function of the $\text{Zn}_{1-x}\text{Sn}_x\text{O}_y$ composition. Adapted with permission from Ref. [83], Copyright (2012) John Wiley & Sons Ltd.

In general, ALD-grown buffer layers for CIGS solar cells have been shown in multiple reports to give comparable conversion efficiencies as CdS. While these ALD layers lead to higher J_{sc} , they rarely outperform traditional CdS in terms of V_{oc} , an effect attributed to higher interface recombination with the alternative buffer layers. The search therefore continues to find compounds that can match or outperform CdS in terms of V_{oc} . In this search, ALD has become a very important tool due to its ability to control material properties of ever more complex compounds. Moreover, the ability to tune the electronic properties of the buffer layer has also spurred interest for ALD among groups currently developing novel crystalline thin film absorber materials as $\text{Cu}_2(\text{Zn},\text{Sn})(\text{S},\text{Se})_4$ [85], SnS [86] and Cu_2O [87], where similar challenges arise as in the CIGS case.

ALD in energy storage: Pt and YSZ for solid oxide fuel cells

Another application in which ALD shows good potential is in next-generation fuel cells, particularly solid oxide fuel cells (SOFCs). SOFCs are solid-state electrochemical devices capable of converting chemical energy, in the form of hydrogen or other hydrocarbon gases, into electrical energy. SOFCs generally consist of three layers – a porous anode material, an ion conducting electrolyte, and a cathode material, all of which can utilize the benefits of ALD. Operating temperatures for typical SOFC devices are 800–1000 °C. Much of the current research into SOFCs is focused on reducing the operating temperatures to ranges between 300 and 600 °C [88–96]. To mitigate limitations associated with lower temperatures, such as lower ionic conductivity and slower reaction kinetics at the electrodes, different strategies have been employed. One approach is to reduce the resistance of the electrolyte, either through the synthesis of a material that has a higher ionic conductivity at lower temperature ranges (300–600 °C) or by reducing the electrolyte film thickness [88,89,92–96]. The latter method offers a two-fold advantage: besides the lower resistance of the device, the thin film allows for rapid ion transfer between electrodes due to the decreased diffusion length [97]. Another approach is to enhance the reaction kinetics at the electrodes with catalysts that are effective at lower temperatures. Both of these approaches can benefit from the advantages imparted by ALD, and a number

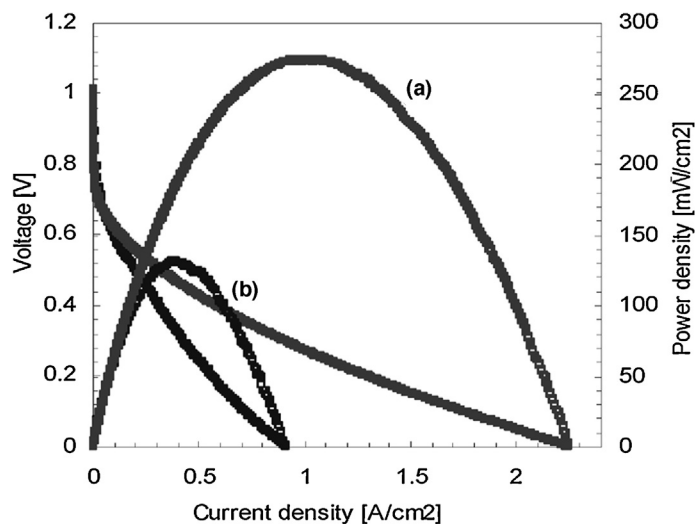


FIGURE 8

Polarization curves and power density of YSZ fuel cells. Performance comparison of (a) ALD YSZ fuel cells to (b) reference fuel cells with 50 nm RF-sputtered YSZ at 350 °C [92]. Adapted with permission from Ref. [92], Copyright (2007) American Chemical Society.

of studies have applied ALD to deposit both electrolytes and catalysts.

The electrolyte in SOFCs is generally yttria stabilized zirconia (YSZ) or gadolinia-doped ceria (GDC), which are dense, ion-conducting ceramics. Several studies have investigated growth of YSZ by ALD, with focus on both improving ionic conductivity and significantly reducing the electrolyte film thickness. YSZ electrolyte has been deposited by alternating ZrO_2 and Y_2O_3 ALD depositions to reach the desired YSZ composition [92,94,98]. In a study by Shim *et al.*, YSZ thin films prepared by ALD were compared to reference films of YSZ prepared by radio frequency (RF) sputtering. $\text{ZrO}_2:\text{Y}_2\text{O}_3$ composition ratios of the YSZ were at 0.92:0.08 (8 mol% Y dopant), a value often targeted for the bulk composition of YSZ for optimal results in SOFCs [94,98,99]. Electrodes for both ALD and RF-sputtered SOFCs were 80 nm of porous Pt. It was demonstrated that 60 nm ALD YSZ films had a power density of 270 mW/cm^2 and activation energy of 0.88 eV, while 50 nm RF sputtered YSZ films had a power density of only 130 mW/cm^2 at 350 °C, as shown in Fig. 8. Additionally, Shim noted that the exchange current density of the ALD-YSZ/Pt interface was four orders of magnitude greater than reference YSZ/Pt interfaces, suggesting the nanocrystalline morphology of the YSZ ALD films enhances the catalytic properties of oxygen dissociation [92].

More recently, investigations of YSZ thin films deposited by ALD have looked at the composition of the YSZ electrolyte and its effect on ion conductivity and catalytic activity. Son *et al.* investigated the ionic conductivity of ALD-grown YSZ, varying the $\text{ZrO}_2:\text{Y}_2\text{O}_3$ ALD cycle ratios from 1:1 to 6:1 [94]. These cycle ratios and their respective growth rates correlated to a dopant mole ratio ranging from 28.8 to 4.3 mol%. The 4:1 cycle ratio (10.4 mol% Y dopant) resulted in the highest conductivity of all films, which was 2 orders of magnitude greater than bulk YSZ (8 mol% Y dopant). This large difference was attributed to the inhomogeneity of the dopant in the vertical direction of the device that arises from the

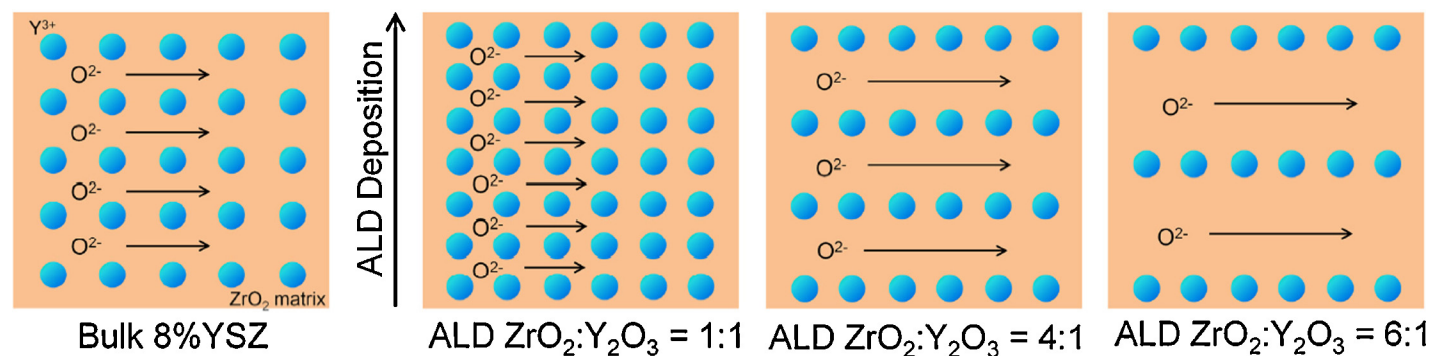


FIGURE 9

Conceptual illustration of dopant ion positioning in bulk YSZ and ALD YSZ films [94]. Reprinted (adapted) with permission from Ref. [94], Copyright (2009) American Vacuum Society.

cyclic nature of the ALD process. This is demonstrated in Fig. 9, where yttria dopants (blue dots) vary spatially in the vertical direction, depending on the ALD cycle ratio. Theoretical evaluation of the spatial doping and its relation to ionic conductivity are currently being investigated. In a related study by Chao *et al.* [98], a surface modification layer (7 nm) of YSZ deposited onto bulk YSZ (500 μm) was investigated for its surface exchange and transport properties. Films deposited with a 2:6 ratio of $\text{Y}_2\text{O}_3:\text{ZrO}_2$ ALD cycles (14 mol% Y dopant) resulted in a fivefold increase in the surface exchange coefficient over bulk YSZ. However, none of the films exhibited improved transport properties.

In addition to electrolyte studies using ALD, much effort has been focused on catalyzing the oxidation and reduction reactions at the electrodes. With reaction activation dropping with operating temperature, many strategies to enhance the reaction kinetics have been investigated. A popular method has been through sputtered and ALD deposited Pt metal for the cathode [90,91]. Pt can be deposited via ALD by (methylcyclopentadienyl) trimethylplatinum (MeCpPt-Me_3) precursor and an air (oxygen) counter reactant. Pt-ALD is typically performed around 275–300 °C. Pt-ALD and noble metal ALD, in general, suffer from slow nucleation rates. However, one of the advantages to using ALD to deposit Pt over sputtering is the intrinsic deposition roughness of noble metal ALD processes, which increases the surface area (triple phase boundary) of the catalyst, leading to a more efficient device [91].

An early study from Jiang *et al.* of Pt electrode catalysts highlighted the opportunity for Pt thin films in SOFCs [90]. In their investigation, the thickness of ALD-grown Pt was varied between 5 nm, 10 nm, and 30 nm and compared to films of 80 nm of Pt deposited via direct current (dc)-sputtering. With the ALD films, maximum catalytic electrode performance was found with 10 nm thick Pt at 50 mW/cm^2 , but 80 nm dc-sputtered Pt films had a higher power density of 80 mW/cm^2 at an operating temperature of 350 °C. This is likely due to the differences in porosity of the two deposition methods. The 10 nm ALD film had porosities in the range of 15–20% while the dc-sputtered films had porosities between 30 and 40%, allowing better fuel diffusivity. Significantly, their study showed that ALD fabrication reduced the Pt loading needed in the SOFC. More recently, An *et al.* [91] investigated the triple phase boundary density of ALD films as a function of ALD cycles and their resulting power density. These ALD thin films were also compared to 80 nm dc-sputtered Pt films. Their results were

consistent with those of Jiang *et al.* and showed that while device improvement was not significant, Pt loading was significantly decreased. The ALD Pt films only required roughly 10% of the Pt metal that dc-sputtered films required for similar device performance. This reduced Pt loading originated from the contiguity and the high triple phase boundary density, as TEM analysis indicated. The reduced loading is a critical finding for the long term economical prospects of using Pt catalysts for microscale SOFCs.

In another study, Jiang *et al.* [100] utilized area-selective ALD processes to create Pt current collector grids on a $\text{La}_{0.6}\text{Sr}_{0.4}\text{Co}_{0.2}\text{Fe}_{0.8}\text{O}_3$ cathode. To generate the grid pattern, microcontact printing methods were utilized, along with an octadecyltrichlorosilane (ODTS) monolayer. ODTS has been shown in previous studies to deactivate the surface for Pt ALD processes [101]. This allowed the Pt metal to be patterned into a grid structure. Power densities of $\mu\text{-SOFC}$ with and without the Pt grid were 110.7 and 11.2 $\mu\text{W}/\text{cm}^2$, respectively. This order of magnitude increase is credited to the enhanced oxygen dissociative adsorption onto the cathode from the Pt metal along with the collection of more current from the cathode.

In summary, ALD techniques have shown great promise in matching performance of sputtered SOFC devices, with the advantage of reducing material loading required for a specific performance. As more is understood about the structure and triple phase boundary of the cathode catalysts and ion conducting electrolytes, ALD, with its excellent composition and thickness control, has the potential to play a pivotal role in the development of next generation SOFCs.

Summary/outlook

With devices becoming ever smaller and increasingly structured into complex three dimensional shapes, the need for controllable and conformal thin films has never been greater. ALD, with its sequential self-limiting reactions, is able to meet these demands in one of the most effective methods possible. Comparable techniques, such as CVD and PVD, cannot always provide the same level of uniformity, conformality and thickness control at the Angstrom level. Because of the advantages of ALD, ALD processes have been developed for a wide variety of materials, ranging from metals to metal oxides to complex ternary materials, allowing ALD to become incorporated into industrial procedures.

In this review, we briefly highlighted many of the advantages of ALD, such as conformality, thickness control, and composition control, along with a broad range of applications in which ALD can be utilized. These applications encompass different technologies, such as the energy conversion industry (photovoltaics, fuel cells) and the semiconductor industry (high-k transistors). In CIGS solar cell devices, ALD has been used to deposit conformal thin films of $Zn_{1-x}Sn_xO_y$ buffer layers. By tailoring the composition and thickness of the $Zn_{1-x}Sn_xO_y$ films via ALD, the device efficiency could be maximized at 18% for an approximate value of $x = 0.20$. For SOFCs, ALD has been utilized in Pt catalyst deposition, showing comparable power densities of devices with dc-sputtered Pt, but requiring only 10% of the Pt metal thickness. Additionally, ALD has been used to deposit thin films of YSZ electrolyte in an effort to reduce the ion exchange distance. By manipulating the $Y_2O_3:ZrO_2$ ratio in ALD super cycles, the composition of the resulting YSZ films can be controlled to provide superior surface exchange and transport properties. Finally, this review showcased emerging high-k dielectric materials, for which ALD has been used to deposit new materials such as Al doped TiO_2 , $LaLuO_3$, $Hf_{1-x}Zr_xO_2$, $SrRuO_3$, and $HfTiO_x$. Also, as transistors have evolved, traditional high-k dielectric ALD procedures, such as that for HfO_2 , have been incorporated for use with FinFETs, providing a uniform and conformal coating on the fin.

As these devices continue to develop, a general emerging trend is the shift from traditional two dimensional planar devices to highly ordered three dimensional structures, often to maximize surface areas and densities to improve the device efficiency. As researchers push the envelope for these smaller complex structures, the demand for precise deposition techniques has never been higher, leading the way for ALD to play an integral role in further device development. With newer technologies like spatial ALD, which allows for faster deposition speeds, and commercially available ALD reactors, the presence of ALD in manufacturing will continue to increase as more materials systems are developed. As the number of ALD systems grows, look for ALD to expand not only in the industries reviewed in this article, but into newer, novel applications such as the medical industry, used for example, in functionalized pharmaceuticals or implanted detectors, and tribology, used for example to create super durable coatings on various surfaces, as well as many others that can benefit from its unique and precise control over thickness, composition, and conformality.

Acknowledgments

This work was supported by the U.S. Department of Energy, Office of Science, Basic Energy Sciences, under Award # DE-SC0004782. The authors also acknowledge fellowship support by the J. Hewes Crispin and Marjorie Holmes Crispin Stanford Graduate Fellowship (RWJ) and the Marcus and Amalia Wallenberg Foundation under the Stig Hagstöm Stipend (AH).

References

- [1] S.M. George, *Chem. Rev.* 110 (1) (2009) 111–131.
- [2] M. Knez, K. Nielsch, L. Niinistö, *Adv. Mater.* 19 (21) (2007) 3425–3438.
- [3] M. Leskelä, M. Ritala, *Angew. Chem. Int. Ed.* 42 (45) (2003) 5548–5554.
- [4] R.L. Puurunen, *J. Appl. Phys.* 97 (12) (2005), 121301-121301-52.
- [5] V. Miikkulainen, et al. *J. Appl. Phys.* 113 (2) (2013), 021301-1–021301-101.
- [6] H. Kim, *J. Vac. Sci. Technol. B: Microelectron. Nanometer Struct.* 21 (6) (2003) 2231–2261.
- [7] M. Leskelä, M. Ritala, *Thin Solid Films* 409 (1) (2002) 138–146.
- [8] J.A. An Delft, D. Garcia-Alonso, W.M.M. Kessels, *Semicond. Sci. Technol.* 27 (7) (2012) 074002.
- [9] T.J. Knisley, L.C. Kalutarage, C.H. Winter, *Coord. Chem. Rev.* 257 (23–24) (2013) 3222–3231.
- [10] J.R. Bakke, et al. *Nanoscale* 3 (9) (2011) 3482–3508.
- [11] T. Suntola, J. Antson, inventors, Method for producing compound thin films, Patent 4058430, November 15, 1977.
- [12] M. Ritala, J. Niinistö, *Chemical Vapour Deposition: Precursors, Processes and Applications*, Royal Society of Chemistry, 2009.
- [13] A. Hultqvist, M. Edoff, T. Törndahl, *Prog. Photovoltaics Res. Appl.* 19 (4) (2011) 478–481.
- [14] A. Kosola, et al. *Appl. Surf. Sci.* 211 (1) (2003) 102–112.
- [15] M. Vehkamäki, et al. *Electrochem. Solid-state Lett.* 2 (10) (1999) 504–506.
- [16] S.D. Elliott, O. Nilsen, *ECS Trans.* 41 (2) (2011) 175–183.
- [17] H. Wang, et al. *Electrochem. Solid-State Lett.* 12 (4) (2009) G13–G15.
- [18] A. Van Gorkum, K. Nakagawa, Y. Shiraki, *J. Appl. Phys.* 65 (6) (1989) 2485–2492.
- [19] F. Werner, et al. *Appl. Phys. Lett.* 97 (2010) 162103.
- [20] P. Poedt, et al. *J. Vac. Sci. Technol. A* 30 (1) (2012), 010802-010802-11.
- [21] D.H. Levy, S.F. Nelson, D. Freeman, *J. Display Technol.* 5 (12) (2009) 484–494.
- [22] D.H. Levy, et al. *Appl. Phys. Lett.* 92 (19) (2008), 192101-192101-3.
- [23] P. Poedt, et al. *Adv. Mater.* 22 (32) (2010) 3564–3567.
- [24] P. Poedt, et al. *J. Electrochem. Soc.* 158 (9) (2011) H937–H940.
- [25] J. Hämäläinen, et al. *Chem. Mater.* 24 (1) (2011) 55–60.
- [26] J. Yum, et al. *J. Appl. Phys.* 109 (6) (2011), 064101-064101-4.
- [27] K. Uusi-Esko, M. Karppinen, *Chem. Mater.* 23 (7) (2011) 1835–1840.
- [28] I. Povey, et al. *Appl. Phys. Lett.* 89 (10) (2006), 104103-1–104103-3.
- [29] H.B. Park, et al. *J. Appl. Phys.* 94 (2003) 3641.
- [30] V. Pore, et al. *J. Am. Chem. Soc.* 131 (10) (2009) 3478–3480.
- [31] S. Ha, E. Choi, S. Kim, *Thin Solid Films* 476 (2) (2005) 252–257.
- [32] J.S. Lim, et al. *ICVC '99 6th International Conference, 1999*, 506–509.
- [33] C. Auth, et al. *2012 Symposium on VLSI Technology (VLSIT), 2012*, 131–132.
- [34] K. Mistry, et al. *Electron Devices Meeting 2007, IEDM 2007, IEEE International, 2007*, pp. 247–250.
- [35] K.J. Kuhn, *IEEE Trans. Electron Dev.* 59 (7) (2012) 1813–1828.
- [36] S. Hyun, et al. *2011 Symposium on VLSI Technology (VLSIT), 2011*, 32–33.
- [37] S. Narasimha, et al. *Electron Devices Meeting (IEDM), 2012 IEEE International, 2012*, 3.3.1–3.3.4.
- [38] F. Koehler, et al. *IOP Conference Series: Materials Science and Engineering*, vol. 41(1), 2012, . p. 012006.
- [39] C.H. Tsai, et al. *2012 International Symposium on VLSI Technology Systems and Applications (VLSI-TSA), 2012*, 1–2.
- [40] F.-L. Yang, et al. *Electron Devices Meeting, 2002 IEDM '02 International, 2002*, 255–258.
- [41] J.-T. Park, J. Colinge, C.H. Diaz, *IEEE Electron Dev. Lett.* 22 (8) (2001) 405–406.
- [42] S. Bangsaruntip, et al. *2010 Symposium on VLSI Technology (VLSIT), 2010*, 21–22.
- [43] V. Elshocht, *Electron Devices Meeting 2008, IEDM 2008, IEEE International, 2008*, 1–4.
- [44] Z.-Y. Xie, et al. *2012 IEEE 11th International Conference on Solid-State and Integrated Circuit Technology (ICSICT), 2012*, 1–3.
- [45] S. Shen, et al. *Appl. Phys. Lett.* 98 (17) (2011), 172902-1–172902-3.
- [46] C.K. Chiang, et al. *Reliability Physics Symposium (IRPS), 2012 IEEE International, 2012*, GD.3.1–GD.3.4.
- [47] J. Hwan Han, et al. *Semiconductor Device Research Symposium (ISDRS), 2011 International, 2011*, 1–2.
- [48] K. Tomida, et al. *IOP Conference Series: Materials Science and Engineering*, vol. 8(1), 2010, . p. 012023.
- [49] C.-W. Chen, et al. *IEEE Electron Dev. Lett.* 33 (12) (2012) 1678–1680.
- [50] B. Liu, et al. *IEEE Trans. Electron Dev.* 60 (6) (2013) 1852–1860.
- [51] M. Radosavljevic, et al. *Electron Devices Meeting (IEDM), 2010 IEEE International, 2010*, 6.1.1–6.1.4.
- [52] P.D. Ye, *J. Vac. Sci. Technol. A* 26 (4) (2008) 697–704.
- [53] M. Radosavljevic, et al. *Electron Devices Meeting (IEDM), 2009 IEEE International, 2009*, 1–4.
- [54] S. Siddiqui, et al. *ECS Trans.* 53 (3) (2013) 137–146.
- [55] R.M. Wallace, et al. *MRS Bull.* 34 (7) (2009) 493.
- [56] W. Wang, et al. *Microelectron. Eng.* 88 (7) (2011) 1061–1065.
- [57] B. Fallahazad, et al. *Appl. Phys. Lett.* 100 (9) (2012) 093112.
- [58] H. Fang, et al. *Nano Lett.* 12 (7) (2012) 3788–3792.
- [59] A.D. Franklin, et al. *Nano Lett.* 13 (6) (2013) 2490–2495.

- [60] L.-J. Chen, et al. *IEEE Trans. Nanotechnol.* 10 (2) (2011) 260–265.
- [61] J. Benick, et al. *Appl. Phys. Lett.* 92 (25) (2008), 253504-1–253504-3.
- [62] H. Schmidt, et al. *Appl. Phys. Lett.* 96 (24) (2010), 243305-1–243305-3.
- [63] E. Palomares, et al. *J. Am. Chem. Soc.* 125 (2) (2003) 475–482.
- [64] K. An, et al. *J. Nanosci. Nanotechnol.* 8 (9) (2008) 4856–4859.
- [65] A.B.F. Martinson, et al. *Appl. Phys. Lett.* 94 (12) (2009), 123107-1–123107-3.
- [66] N.P. Dasgupta, et al. *Nano Lett.* 11 (3) (2011) 934–940.
- [67] T.P. Brennan, et al. *Adv. Energy Mater.* 1 (6) (2011) 1169–1175.
- [68] M. Kapilashrami, et al. *Phys. Chem. Chem. Phys.* 14 (29) (2012) 10154–10159.
- [69] S. Niki, et al. *Prog. Photovoltaics Res. Appl.* 18 (6) (2010) 453–466.
- [70] A. Niemegeers, M. Burgelman, A. De Vos, *Appl. Phys. Lett.* 67 (6) (1995) 843–845.
- [71] J. Lindahl, et al. *Prog. Photovoltaics Res. Appl.* 21 (8) (2013) 1588–1597.
- [72] N. Naghavi, et al. *Prog. Photovoltaics Res. Appl.* 18 (6) (2010) 411–433.
- [73] V. Lujala, et al. *Appl. Surf. Sci.* 82–83 (0) (1994) 34–40.
- [74] E.B. Yousfi, et al. *Thin Solid Films* 361–362 (0) (2000) 183–186.
- [75] T. Törndahl, et al. *Prog. Photovoltaics Res. Appl.* 15 (3) (2007) 225–235.
- [76] N. Naghavi, et al. *Prog. Photovoltaics Res. Appl.* 11 (7) (2003) 437–443.
- [77] K. Ramanathan, et al., Comparative Study of Zn(O,S) Buffer Layers and CIGS Solar Cells Fabricated By CBD, ALD, and Sputtering, (2012) NREL Report No. CP-5200-54138.
- [78] T. Nakada, et al. *IEEE J. Photovoltaics* 3 (1) (2013) 461–466.
- [79] N. Naghavi, et al. *Thin Solid Films* 519 (21) (2011) 7600–7605.
- [80] K. Nakashima, et al. *Jpn. J. Appl. Phys.* 51 (2012), 10NC15.
- [81] C. Lee, Y.M. Shin, B.T. Ahn, *ECS Trans.* 41 (4) (2011) 213–219.
- [82] J. Rousset, et al. *Sol. Energy Mater. Sol. Cells* 95 (6) (2011) 1544–1549.
- [83] A. Hultqvist, et al. *Prog. Photovoltaics Res. Appl.* 20 (7) (2012) 883–891.
- [84] P. Genevee, et al. *J. Vac. Sci. Technol. A* 31 (1) (2013) 01A131.
- [85] D.A.R. Barkhouse, et al. *Appl. Phys. Lett.* 100 (19) (2012), 193904-1–193904-5.
- [86] P. Sinsermsuksakul, et al. *Appl. Phys. Lett.* 102 (5) (2013), 053901-1–053901-5.
- [87] Y. Lee, et al. *Energy Environ. Sci.* 6 (2013) 2112–2118.
- [88] D. Beckel, et al. *J. Power Sources* 173 (1) (2007) 325–345.
- [89] H. Huang, et al. *J. Electrochem. Soc.* 154 (1) (2007) B20–B24.
- [90] X. Jiang, et al. *Chem. Mater.* 20 (12) (2008) 3897–3905.
- [91] J. An, Y. Kim, F.B. Prinz, *Phys. Chem. Chem. Phys.* 15 (20) (2013) 7520–7525.
- [92] J.H. Shim, et al. *Chem. Mater.* 19 (15) (2007) 3850–3854.
- [93] C. Brahim, et al. *Appl. Surf. Sci.* 253 (8) (2007) 3962–3968.
- [94] K. Sik Son, et al. *J. Vac. Sci. Technol. A* 31 (1) (2013), 01A107-1–01A107-4.
- [95] J.H. Shim, et al. *Chem. Mater.* 21 (14) (2009) 3290–3296.
- [96] C. Bernay, et al. *J. Phys. Chem. Solids* 64 (9) (2003) 1761–1770.
- [97] A. Evans, et al. *J. Power Sources* 194 (1) (2009) 119–129.
- [98] C. Chao, et al. *ACS Nano* 7 (3) (2013) 2186–2191.
- [99] B. Steele, *Solid State Ionics* 75 (1995) 157–165.
- [100] X. Jiang, R. Chen, S.F. Bent, *Surf. Coat. Technol.* 201 (22) (2007) 8799–8807.
- [101] R. Chen, S.F. Bent, *Adv. Mater.* 18 (8) (2006) 1086–1090.